Wuhan University
Journal of Natural Sciences

2019, Vol.24 No.3, 257-270

Article ID 1007-1202(2019)03-0257-14
DOI https://doi.org/10.1007/s11859-019-1395-5

Susceptibility Assessment of Landslides in Alpine-Canyon Region Using Multiple GIS-Based Models

☐ **HU Man[1], LIU Qiuqiang[2], LIU Pengyu[1]**

1. College of Engineering and Technology, Southwest University, Chongqing 400715, China;

2. Consultative Centre for Geo-Hazard Emergency, Ministry of Land and Resources of China, Beijing 100081, China

Abstract: This study explores a comparative study of three susceptibility assessment models based on remote sensing (RS) and geographic information system (GIS). The Lenggu region (China) was selected as a case study. At first, a landslide inventory map was compiled using data from existing geology reports, satellite imagery, and coupling with field observations. Subsequently, three models were built to map the landslide susceptibility using analytical hierarchy process (AHP), fuzzy logic (FL) and certainty factors (CF). The resulting models were validated and compared using areas under the curve (AUC). The AUC plot estimation results indicated that the three models are promising methods for landslide susceptibility mapping. Among the three methods, CF model has highest prediction accuracy than the other two models. Similarly, the outcome of this study reveals that streams, faults, slope and elevation are the main conditioning factors of landslides. Especially, the erosion of streams plays a key role of the landslide occurrence. These landslide susceptibility maps, to some extent, reflect spatial distribution characteristics of landslides in alpine-canyon region of southwest China, and can be used for land planning and hazard risk assessment.

Key words: landslide; susceptibility assessment; geographic information system (GIS); analytical hierarchy process (AHP); fuzzy logic (FL); certainty factors (CF)

CLC number: TP 305

Received date: 2018-07-28

Foundation item: Supported by the National Natural Science Foundation of China (41602354), the Chongqing Research Program of Basic Research and Frontier Technology (2017jcyjAX0300), and the Fundamental Research Funds for the Central Universities (XDJK2016B027)

Biography: HU Man, female, Lecturer, research direction: natural disaster modelling and analysis. E-mail: humanyyyes@126.com

0 Introduction

Landslides are very common in the alpine-gorge terrain of southwest China, due to a combination of steep topography, high tectonic uplift rates, poor vegetation, heavy precipitation and seismic activity[1,2]. Millions of cubic meters of material of landslides usually involve and inflict severe damages to infrastructure, properties and loss of life[3].

The magnitude, the frequency of occurrence and the impact on human activity of historical landslides and debris flows in southwest China have motivated many studies of different aspects of landslides[4-8]. Among these studies, understanding landslide mechanisms and mapping susceptible areas are essential for land use planning, as well as supports for decision-making activities in this area. However, exploring a suitable and reliable model for landslide susceptibility assessment is still challenging due to the complex nature of landslides. Meanwhile, both the quality of relevant spatial datasets and the employed models have close impact on the susceptibility mapping and assessment[9-11]. To address this, various methods and techniques have been proposed for the susceptibility analysis of or landslides or debris flows, furthermore, to understand the controlling factors and to predict the spatial distribution of landslides[12-19]. Among these models, statistical-based and physical-based approaches are the most used methods. Physical-based techniques focus on the influence of geotechnical characteristics on susceptibility analysis, which are suitable for small or well-monitored landslides to investigate physical, mechanical, and hydrological factors[11], thus

these models are not efficient, economical and practical for large-scale areas.

Statistical-based models and machine learning models assume conditions that caused slope failure in the past and present are the same as those which are likely to cause landslides in the future. In the literatures, the most common statistical and machine learning models used in landslide modeling are logistic regression[20], discriminant analysis[21], fuzzy logic[22] artificial neural networks[23] and support vector machines[24] etc. Over the past decades, geographic information system (GIS), global positioning system (GPS) and remote sensing (RS) have been widely used in geological hazard risk assessment[25]. Compared with the traditional means of landslide survey, the inventory of landslides in the area that human can rarely reach is relatively easy to access with the availability of satellite imagery and aerial photography.

In this paper, the analytical hierarchy process (AHP), fuzzy logic (FL) and certainty factors (CF) techniques were used to analyze landslide susceptibility in the Lenggu Dam site area. These models have been evaluated and compared. Eight major factors, namely, elevation, hill slope, slope aspect, lithology, distance to faults, distance to streams, distance to roads and normalized difference vegetation index (NDVI), were selected for landslide susceptibility analysis. The weights of the conditioning factors and certainty factors were obtained by the three models, respectively. The received operating characteristics (ROC) was eventually used for the assessment, validation, and comparison of the resulting models in order to choose the best model in this study.

1 Study Area

In this work, susceptibility analysis of landslides was conducted in the Lenggu Dam site area. The Lenggu Hydropower Station is the third cascade hydropower project in the middle reach of the Yalong River, which is a southward-flowing tributary of the Jinsha River in Sichuan, southwest China. The station controls a basin area of 77 543 km^2, which occupies 57% of the Yalong River. The whole Lenggu Dam site area is located partly in Yajiang County and partly in Kangding County, Sichuan Province (Fig. 1).

Located in the east edge of Tibetan Plateau, the study area is strongly affected by the ongoing plate convergence between India and Eurasia. Hence, the Yalong River was eroding downward to form the canyon with quite steep slopes with uplifting of crust in the Quaternary[26]. As a result of the unloading from the river incision, the rocks on the both sides of valleys are heavily fractured and eroded. Landslides, rock falls or rockslides were formed and they brought huge amounts of deposit onto the bed rock surface[27]. Such a large deposit exhibits a complex record of instability, which is possible to pose problems during engineering construction.

Fig. 1 Location of study area

1.1 Geological Settings

Based on the field investigation, the study area is a region underlain by metamorphic rocks. Four main faults are located in the dam site (Fig. 2). Dahaizi, Milong, Songyu and Caiyu faults are notable because of their

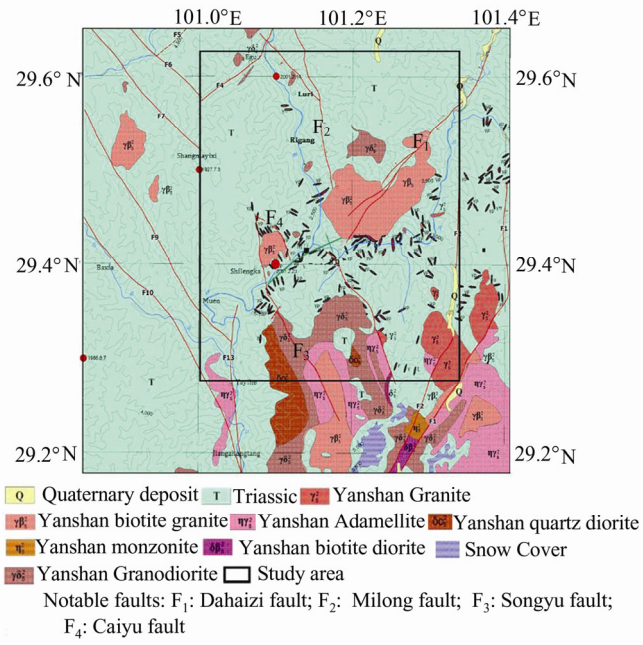

Fig. 2 Geology of the dam area

intense activities. The bedrock exposed in this area is primarily the Triassic Formation, which consists of metasandstone and slate. The metasandstone is gray and fine-to-medium grained. Quartz dikes, generally following fractures and bedding, are associated with the metasandstone.

According to the history of the regional seismic records near Yalong River, several strong earthquakes have been triggered by the faults nearby in the dam area. Among 91 earthquakes, those MS≥4.7 were recorded by the end of June 2008. The magnitude of the earthquakes is shown in Fig. 3.

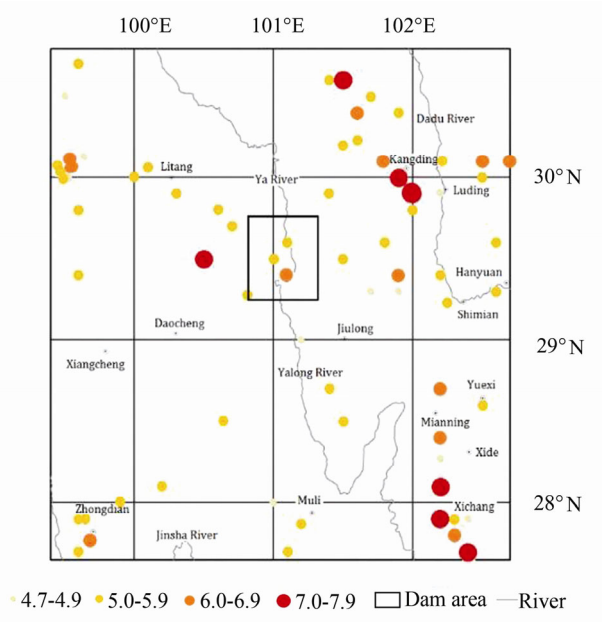

Fig. 3 Earthquake of MS≥4.7 epicenter distribution in the dam area

1.2 Topography

In the study area, elevation of mountains ranges from 4 600 to 4 900 m. The Yalong River flows from north to south. Figure 4 shows the field photographs of Yahong River. The cutting depth of the river is deeper in the lower reaches than in the upper reaches. Slope gradients of the mountains reach 40º-55º in the lower reaches, and 30º-40º in the upper reaches. Slope gradients of several hills reach 60º-85º, forming a V shape. It is a typical alpine canyon landscape.

(a) Upper reaches of Yalong River (b) Lower reaches of Yalong River

Fig. 4 Field photographs of Yahong River

1.3 Meteorology

In southwest China, there is an alpine-valley region that is usually called a "dry-hot valley". During summer, this particular terrain causes the warm and moist air flow to lose its moisture upon reaching the valleys. However, during winter, dry continental air flow carries less moisture. After thousands of years, these particular phenomenon contribute to the formation of a "dry-hot valley".

The study area, located in the dry-hot valley region, has an annual average temperature about 22 ℃ with recorded temperatures of −2 to 42 ℃. Such temperature difference accelerates weathering of rock masses and generates new loose materials, thus providing conditions for triggering landslides and debris flows.

On average, the study area receives 949.1 mm of rain per year, with most of the precipitation (90%-95%) occurring between May and October. Hourly and daily rainfall thresholds range from 30 to 40 mm, and from 70 to 80 mm, respectively. Therefore, landslides and debris flows are likely to occur in the area[28].

2 Methodologies

2.1 AHP Model

The AHP model is a powerful and practical technique for quantitatively multi-criteria decisions[29]. AHP is considered as a subjective-weighting method for justifying decision optimality based on perceptions and judgments. Since developed, AHP model has been widely used in landslide susceptibility analysis and many studies have been conducted[8].

The AHP needs to check the rationality of the characteristic vector which is based on the judgment matrix, and it asks for that the judgment matrix has the general consistency in order to ensure that the calculation results are basically reasonable. Therefore, it is necessary to test the consistency of the judgment matrix. R_c, named the consistency ratio, is acquired by comparing the consistency index I_c to a random consistency index I_R. The consistency test can be expressed as

$$R_c = \frac{I_c}{I_R} \tag{1}$$

I_c can be expressed as

$$I_c = \frac{\lambda_{max} - n}{n-1} \tag{2}$$

where n is the number of parameters and λ_{max} is the largest eigenvalue of a preference matrix. The smaller R_c, the greater the consistency. The matrix can be accounted as having satisfactory consistency in condition of R_c being less than 0.1[8]. Otherwise, it is necessary to revise and adjust the judgment matrix at this level until the consistency test meets the requirements.

2.2 CF Model

CF model is usually used to evaluate the sensitivity of various factors that affect an event. CF model is a kind of the probability function first proposed by Shortliffe and Buchanan[30]. The CF model is considered as one of the favorable models to deal with the problem of the uncertainty of data layers. Therefore, the CF model has been widely applied to geological disaster susceptibility assessment such as landslide and debris flow susceptibility assessment[31]. The weights of each pixel of maps are classified by applying Eq. (3):

$$\mathrm{CF}=\begin{cases}\dfrac{\mathrm{PP_a}-\mathrm{PP_s}}{\mathrm{PP_a}(1-\mathrm{PP_s})}, & \mathrm{PP_a}\geqslant\mathrm{PP_s}\\ \dfrac{\mathrm{PP_a}-\mathrm{PP_s}}{\mathrm{PP_s}(1-\mathrm{PP_a})}, & \mathrm{PP_a}<\mathrm{PP_s}\end{cases} \tag{3}$$

where CF is the certainty factor. $\mathrm{PP_a}$ is the conditional probability of landslide occurring. $\mathrm{PP_s}$ is the conditional probability of the numbers of landslide in the study area. At a practical level, $\mathrm{PP_a}$ is the ratio of the area of landslides in the study area to the whole research area, and $\mathrm{PP_s}$ is the ratio of the area of landslide occurrence to the total area of the influence factor in a certain level.

In the CF model, an increasing certainty of the landslide occurrence can be expressed by a positive value between [0, 1], while the decreasing certainty of the landslide occurrence can be represented by a negative value within the interval [−1, 0]. A value close to 0 means the certainty of landslide occurrences is not sure, and it is hard to make the judgement. .

Firstly, the CF values of conditioning factors of landslides were calculated through Eq. (4). Then, the calculated CF values were integrated in pairs. The CF value Z is the integral of the two CF values of X and Y which can be determined as follows[32]:

$$Z=\begin{cases}X+Y-XY, & X,Y\geqslant 0\\ \dfrac{X+Y}{1-\min(|X|,|Y|)}, & X*Y<0\\ X+Y+XY, & X,Y<0\end{cases} \tag{4}$$

The pairwise integration is repeated until all layers are calculated and the landslide susceptibility index is finally calculated.

2.3 FL Model

FL was first proposed by American mathematician Zadeh in 1965[33]. The FL model converts the original variables into fuzzy sets represented by membership functions. The interval [−1, 1] of fuzzy sets indicates the true extent of the propositional assertions, which is also called the membership degree.

When the membership degree reaches 1, the area is completely favorable for the landslide disaster, whereas the value of the membership degree close to 0 represents the area is completely not favorable for the landslide disaster at all. With the use of the fuzzy logic method, the variables are usually first blurred. That is to say, the membership degree of the variable is first calculated by the membership function. Fuzzy operators are then combined. The membership degree of this study is calculated as follows:

$$\mu(n_i)=\begin{cases}0, & n_i \quad \mathrm{Min}\\ \dfrac{n_i-\mathrm{Min}}{\mathrm{Max}}, & \mathrm{Min}<n_i<\mathrm{Max}\\ 1, & n_i\geqslant\mathrm{Max}\end{cases} \tag{5}$$

where n_i is the number of landslides in different categories, and $\mu(n_i)$ is the membership function. Max is 90% of the largest n_i value in the category, and Min is 10% of Max.

The fuzzy operator used in the fuzzy synthesis is the γ operator[34], and the γ operator can be written as follows:

$$\mu_{(x)}=\left(\prod_{i=1}^{n}\mu_i\right)^{\gamma}\cdot\left[1-\prod_{i=1}^{n}(1-\mu_i)\right]^{1-\gamma} \tag{6}$$

where μ_i is the membership degree of number i variables; γ has a value between 0 and 1.

3 Data

3.1 Landslide Inventory Map

A landslide inventory map, which identifies the specific location of the existing landslides, is crucial in the work of landslide susceptibility assessments[35,36]. It allows us to figure out the relations between existing landslide with conditioning and triggering, and to acquire the connection between landslides that have occurred in the past and that will take place in future. In the study area, extensive field surveys and observations were conducted to produce a detailed and reliable landslide inventory map. A total of 76 landslides were identified and mapped by using aerial photograph. The satellite images and field survey

and the locations of 76 landslides are mapped in Fig. 5.

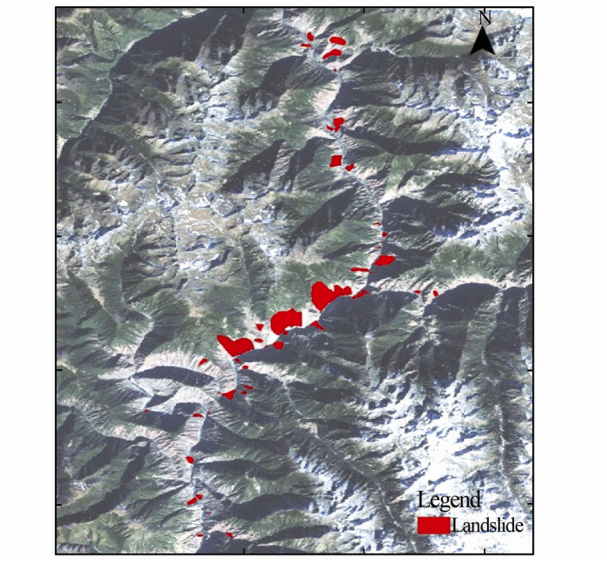

Fig. 5 A landslide inventory map of study area

Some views of the recent landslides identified in the study area are shown in Fig. 6. A digital elevation model (DEM) was created at 1:25 000-sclae. The DEM map has a grid size of 30 m with 15 354 cells.

3.2 Production of the Thematic Data Layers

In order to carry out the landslide susceptibility zoning of the study area, eight landslide conditioning factors were considered. These factors are slope angle, slope aspect, altitude, lithology, distance from faults, distance from rivers, distance from roads and NDVI. AHP model was taken for instance. Eight data layers were produced by the following steps.

• **Slope angle**

The slope angle is the most commonly used parameter in preparing landslide susceptibility maps[37], because the greater downslope component of gravity at steeper slope results in the increase of shear stress in the slope, increasing the probability of landslide occurrence[38]. In this study, the slope angle map of the study area was derived from a DEM with 30 m spatial resolution and divided into eight slope categories (Fig. 7(a)).

• **Slope aspect**

The slope aspect has been considered as an important factor for landslide susceptibility mapping since it can directly affect slope instability[39]. The different slope aspects result in the different exposure to drying winds in ‘‘dry-hot valley’’, sunlight and degree of saturation as a result of rainfall[40]. In this study, slope aspects were grouped into eight classes, shown as flat, north (N, 337.5°- 360°, 0°-22.5°), northeast (NE, 22.5°-67.5°), east (E, 67.5°-112.5°), southeast (SE, 112.5°-157.5°), south (S, 157.5°-202.5°), southwest (SW, 202.5°-247.5°), west (W, 247.5°-292.5°) and northwest (NW, 292.5°-337.5°) in Fig. 7(b).

• **Altitude**

Altitude is widely applied in the analysis of landslide susceptibility. The elevation range of the study area is 2 190-5 200 m, which is divided into eight grades, spacing of 500 m (Fig. 7(c)).

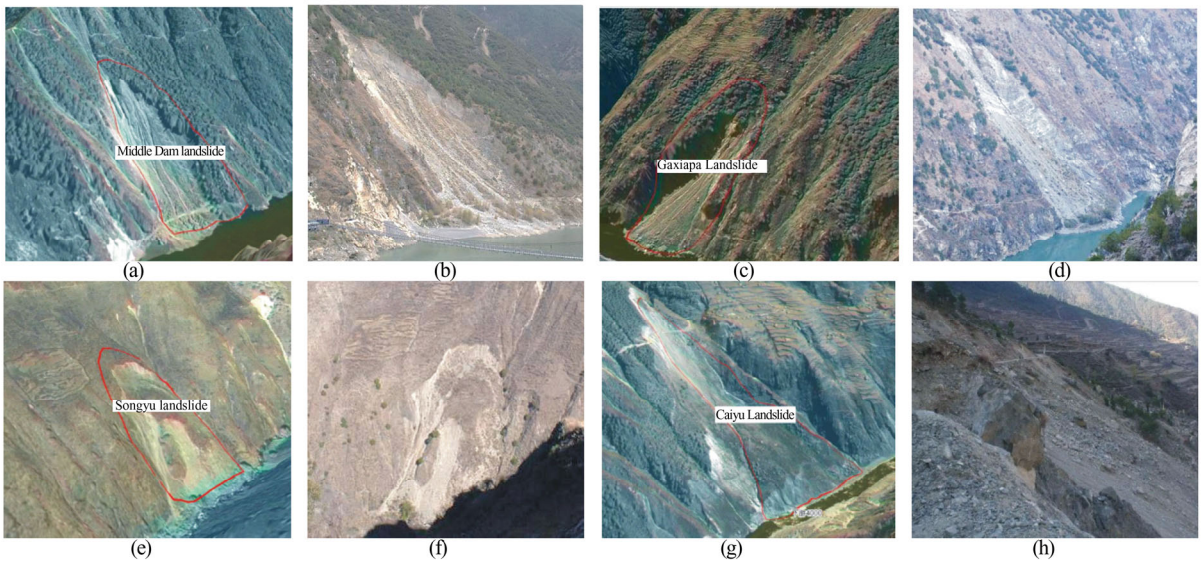

Fig. 6 Images in three-dimensional image system and field photographs of some occurred landslides in study area

(a) Middel Dam Landslide (in three-dimensional image system); (b)Middel Dam Landslide (field photographs); (c) Gaxiapa Landslide (in three- dimensional image system); (d) Gaxiapa Landslide (field photographs); (e) Songyu Landslide (in three-dimensional image system); (f) Songyu Landslide (field photographs); (g) Caiyu Landslide (in three-dimensional image system); (h) Caiyu Landslide (field photographs)

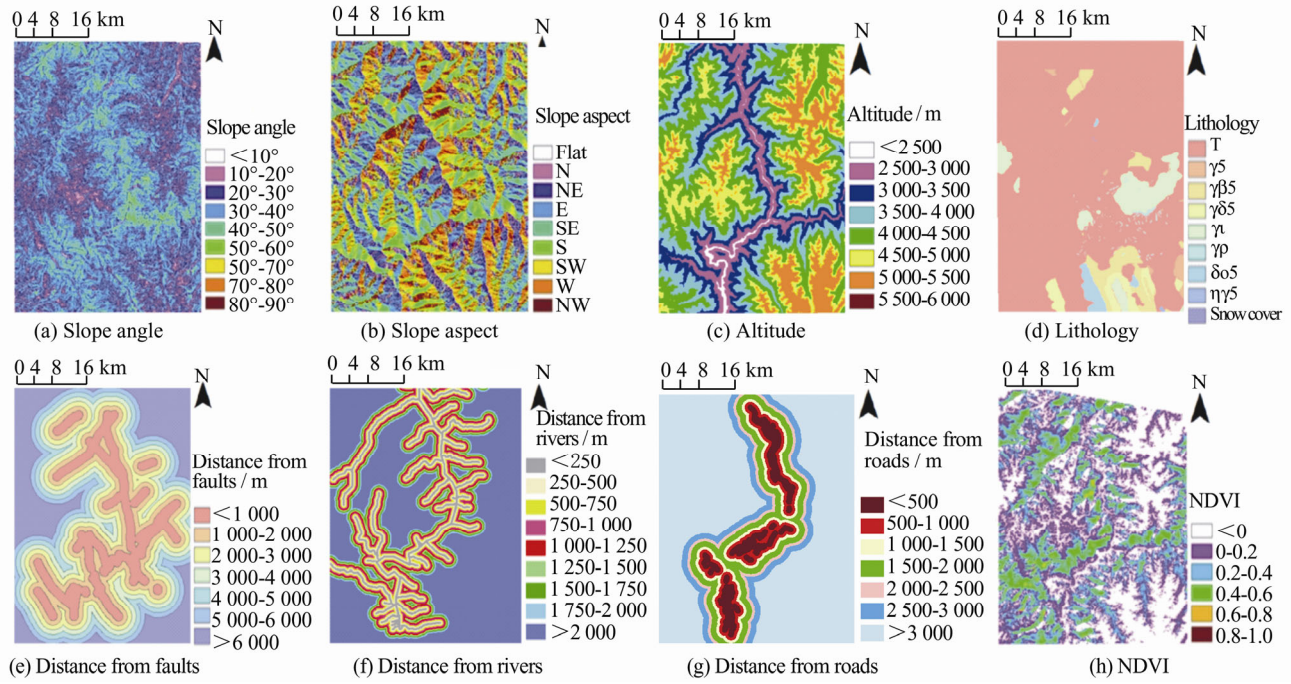

Fig. 7 Landslide conditioning factors of the study area in AHP model

• **Lithology**

Lithology directly reflects the shear strength and permeability of the rock. Different lithological units have different abilities to resist the weathering and erosional processes[41]. Lithology, therefore, is very important in the study of landslide susceptibility[42]. Nine lithological classifications were identified in the study area (Fig. 7(d)).

• **Distance from faults**

Faults are usually related to slope failures[43]. Due to the weak strength of the rock mass by shearing, seismic shaking and other mechanisms nearby faults, a weak line or zone around a fault can be characterized by heavily fractured rocks[44]. Fault lines were obtained from the geological map of the study area. The distances from faults were classified into seven categories with an interval of 1 000 m (Fig. 7(e)).

• **Distance from rivers**

The distance from rivers often affects the channel incision on hillslope processes and landscape evolution[45]. Meanwhile, the moisture saturation of geo-material plays an important role in the slope stability. In this study, nine different buffer zones were produced with a spacing of 250 m (Fig. 7(f)).

• **Distance from roads**

In mountainous region, any road cuttings on natural slopes can cause the initiation of slope mass movements[46]. The distance from roads, therefore, could be helpful to be considered as a conditioning factor in landslide occurrence. The map of distance from roads was also constructed by buffering having the respective interval of 500 m in this paper (Fig. 7(g)).

• **NDVI**

NDVI is a measure of surface reflectance and gives a quantitative estimate of the vegetation growth and biomass[47]. NDVI, derived from the satellite images, was taken into consideration as a landslide-related factor. The NDVIs were calculated by the following equation:

$$\mathrm{NDVI}=\frac{\mathrm{IR}-R}{\mathrm{IR}+R} \tag{7}$$

where IR is the infrared portion of the electromagnetic spectrum; R is the red portion of the electromagnetic spectrum. In this study NDVIs were classified into six groups with an interval of 0.2(Fig. 7(h)).

For CF model and FL model, similar to AHP model, eight data layers were generated according to eight landslide conditioning factors of the study area, which were divided into several categories with a certain interval. The data layers are presented in Figs. 8 and 9.

4 Results and Discussion

4.1 Result of AHP Model

The eight conditioning factors have been ranked respecting the impact to landslide occurrences in Table 1. The last line shows the weight for each factor. Finally, the landslide susceptibility index (LSI) using AHP model is constructed by using the following equation[48] :

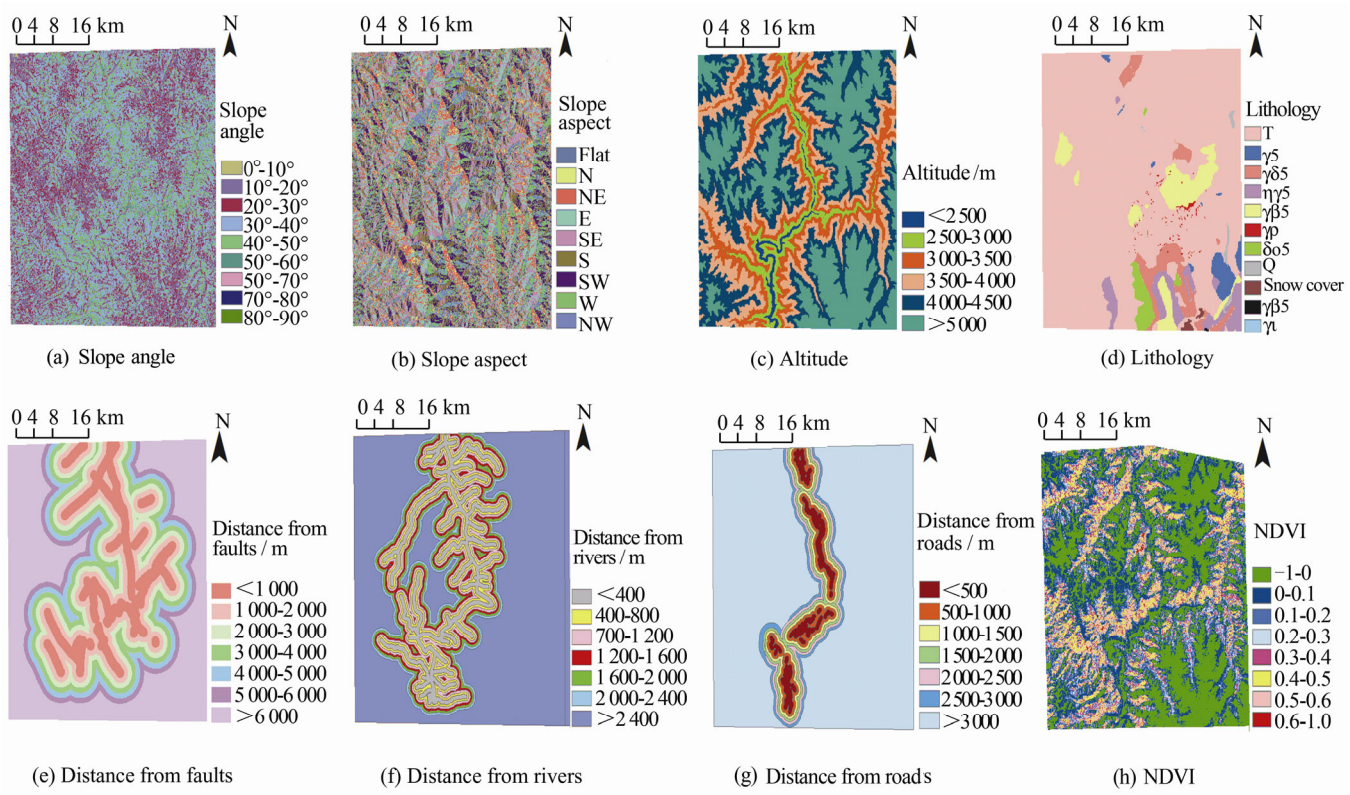

Fig. 8 Landslide conditioning factors of the study area in CF model

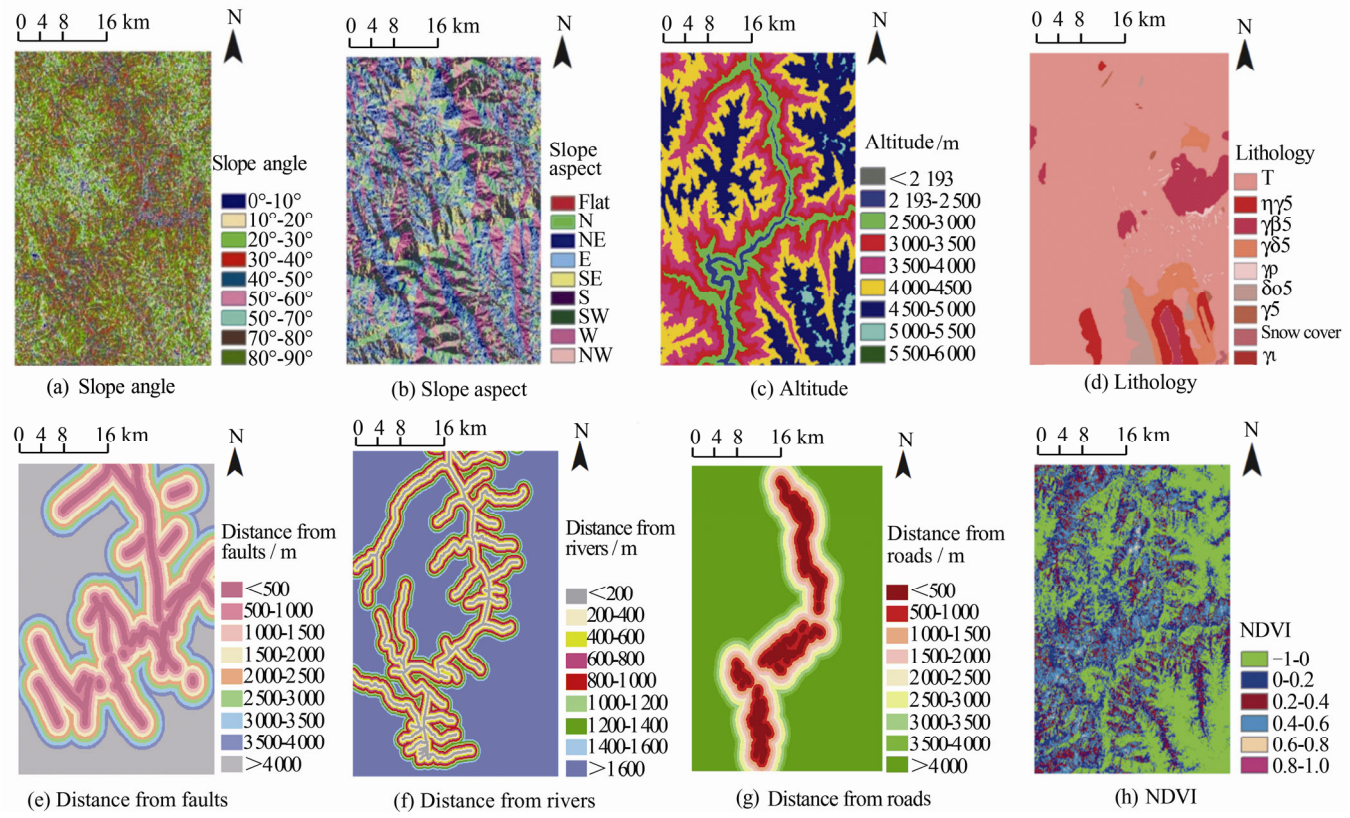

Fig. 9 Landslide conditioning factors of the study area in FL model

$$\begin{aligned}\mathrm{LSI}_{\mathrm{AHP}} &= (\text{slope angle}\times W_{\mathrm{AHP}}) + (\text{slope aspect}\times W_{\mathrm{AHP}}) \\ &+ (\text{altitude}\times W_{\mathrm{AHP}}) + (\text{lithology}\times W_{\mathrm{AHP}}) \\ &+ (\text{distance from faults}\times W_{\mathrm{AHP}}) \\ &+ (\text{distance from rivers}\times W_{\mathrm{AHP}}) \\ &+ (\text{distance from roads}\times W_{\mathrm{AHP}}) + (\text{NDVI}\times W_{\mathrm{AHP}})\end{aligned} \tag{8}$$

where W_{AHP} is the weightage for each landslide conditioning factor. The levels of the influence of conditioning factors were calculated by AHP model (Table 1). According to Table 1, it can be seen that slope angle and slope aspect have the most and less influence on landslide occurrence with values of 0.296 and 0.032, respectively. The other factors such as altitude, lithology, distance from faults, distance from rivers, distance from roads and NDVI have weights of 0.082, 0.222, 0.144, 0.058, 0.053, and 0.111, respectively. The pixel values were then reclassified in five groups by the natural break method (very low, low, moderate, high, and very high). The landslide susceptibility mapping by AHP model is shown in Fig. 10.

Table 1 Paired comparison judgment matrix and the weight of each conditioning factors by analytical hierarchy process

Conditioning factors	(1)	(2)	(3)	(4)	(5)	(6)	(7)	(8)
(1)	1	1/3	3	1/4	7	6	5	1
(2)	3	1	5	1/2	9	7	5	1
(3)	1/3	1/5	1	1/6	6	3	2	1
(4)	4	2	6	1	9	7	7	1
(5)	1/7	1/9	1/6	1/9	1	1/3	1/3	1
(6)	1/6	1/7	1/3	1/7	3	1	3	1
(7)	1/5	1/5	1/2	1/7	3	1/3	2	1
(8)	1	1	1	1	1	1	1	1
Weight	0.144	0.222	0.082	0.296	0.032	0.058	0.053	0.111

Consistency ratio: 0.161; (1) distance from faults; (2) lithology; (3) altitude; (4) slope angle; (5) slope aspect; (6) distance from rivers; (7) distance from roads; (8) NDVI

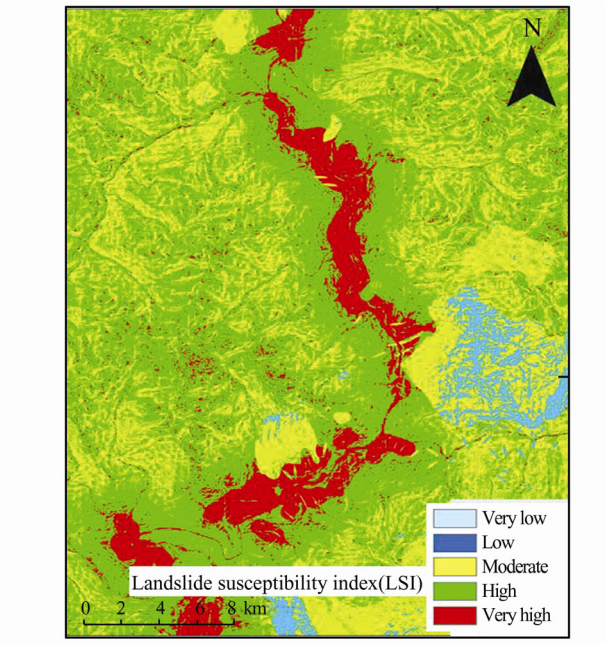

Fig. 10 Landslide susceptibility map derived from the AHP model

4.2 Result of CF Model

By superimposing and calculating the landslide frequency, the CF values of all factors were calculated (Table 2). Then, the CF values of 8 conditioning factors were determined through Eq. (3). The results of spatial relationship between landslide and conditioning factors are presented in Table 2. The CF values of the study area were calculated using Eq. (3) and Eq. (4).

Finally, the LSI values of CF model in the study area are between −1.000 and 0.939. Using natural breaking method, LSI values were divided into five categories (very low, low, moderate, high, and very high).

4.3 Result of FL Model

For FL model, the spatial relationship parameters of eight conditioning factors were calculated through the equations mentioned in Section 2.3. The results of spatial relationship between landslide and conditioning factors are presented in Table 3. The pixel values were then reclassified in five groups by the natural break method (very low, low, moderate, high, and very high).

The landslide susceptibility can be mapped by CF and FL model shown in Figs. 11 and 12, respectively.

Table 2 Spatial relationship between each landslide conditioning factor and landslide by the CF model

Conditioning factors	Classes	Graded total area/km^2	Landslide area/km^2	Percentage of Landslide area/%	CF
Altitude	＜2 500 m	38.340	2.814	7.341	0.939
	2 500-3 000 m	178.259	8.397	4.711	0.902
	3 000-3 500 m	352.906	1.765	0.500	0.041
	3 500-4 000 m	563.118	0.076	0.013	−0.972
	4 000-4 500 m	797.216	0.000	0.000	−1.000
	＞4 500 m	758.821	0.000	0.000	−1.000
Slope angle	＜10°	167.008	0.339	0.203	−0.578
	10°-20°	467.370	1.655	0.354	−0.263
	20°-30°	714.920	3.149	0.440	−0.082
	30°-40°	788.659	4.514	0.572	0.163
	40°-50°	457.676	2.819	0.616	0.222
	50°-60°	113.504	0.542	0.477	−0.005
	60°-70°	10.715	0.023	0.219	−0.545
	70°-80°	0.614	0.010	1.646	0.712
	>80°	0.018	0.000	0.000	−1.000
Slope aspect	Flat	0.061	0.000	0.000	−1.000
	North	320.002	0.235	0.073	−0.848
	Northeast	376.207	0.764	0.203	−0.578
	East	363.214	3.171	0.873	0.453
	Southeast	297.440	3.799	1.277	0.627
	South	306.720	1.696	0.553	0.133
	Southwest	366.221	1.308	0.357	−0.257
	West	350.288	1.331	0.380	−0.209
	North	340.331	0.749	0.220	−0.542
Lithology	T	2 230.476	12.163	0.545	0.145
	γ5	45.708	0.115	0.251	−0.462
	γβ5	151.801	0.015	0.010	−0.979
	γδ5	121.906	0.000	0.000	−1.000
	γι	0.200	0.000	0.000	−1.000
	γρ	9.483	0.294	3.104	0.854
	δβ5	0.510	0.000	0.000	−1.000
	δo5	45.361	0.000	0.000	−1.000
	ηγ5	106.411	0.103	0.097	−0.793
	Snow Cover	6.402	0.000	0.000	−1.000
Distance form faults	＜1 000 m	379.882	5.634	1.483	0.507
	1 000-2 000 m	343.417	5.709	1.662	0.561
	2 000-3 000 m	314.106	1.533	0.488	−0.340
	3 000-4 000 m	279.161	0.022	0.008	−0.990
	4 000-5 000 m	238.003	0.040	0.017	−0.978
	5 000-6 000 m	216.399	0.115	0.053	−0.928
	＞6 000m	1 045.715	0.000	0.000	−1.000

Continued on next page

Table 2 (continued)

Distance from rivers	＜400 m	60.454	4.791	7.925	0.548
	400-800 m	60.272	4.412	7.321	0.508
	800-1 200 m	58.808	2.492	4.237	0.121
	1 200-1 600 m	56.468	0.893	1.581	−0.587
	1 600-2 000 m	56.113	0.461	0.822	−0.787
	2 000-2 400 m	56.671	0.003	0.006	−0.998
	＞2 400 m	1662.138	0.000	0.000	−1.000
Distance from roads	＜500 m	109.627	8.962	8.175	0.705
	500-1 000 m	82.654	2.886	3.491	0.274
	1 000-1 500 m	79.459	0.344	0.432	−0.835
	1 500-2 000 m	80.421	0.450	0.559	−0.786
	2 000-2 500 m	72.085	0.289	0.401	−0.847
	＞3 000 m	85.649	0.123	0.143	−0.945
NDVI	−1-0	1231.672	7.979	0.648	0.250
	0-0.1	439.638	3.744	0.852	0.431
	0.1-0.2	227.556	0.662	0.291	−0.403
	0.2-0.3	203.414	0.234	0.115	−0.765
	0.3-0.4	224.529	0.203	0.090	−0.815
	0.4-0.5	231.928	0.176	0.076	−0.844
	0.5-0.6	95.460	0.047	0.049	−0.899
	0.6-1	14.616	0.007	0.051	−0.897

Table 3 Spatial relationship between each landslide conditioning factor and landslide by the FL model

Conditioning factors	i	n	n_i	$\mu(n_i)$
Altitude	2 193 m	1	0	0
	2 193-2 500 m	41 175	3 258	0.266 5
	2 500-3 000 m	178 121	9 877	1
	3 000-3 500 m	265 189	2 131	0.139 7
	3 500-4 000 m	370 977	88	0
	4 000-4 500 m	475 480	0	0
	4 500-5 000 m	481 267	0	0
	5 000-5 500 m	31 560	0	0
	5 500-6 000 m	6	0	0
Slope angle	0°-10°	110 922	405	0
	10°-20°	308 380	1 899	0.292 5
	20°-30°	471 316	3 670	0.658 5
	30°-40°	540 391	5 376	1
	40°-50°	327 478	3 315	0.585 1
	50°-60°	77 479	648	0.033 9
	60°-70°	7 184	26	0
	70°-80°	605	0	0
	80°-90°	21	0	0

Continued on next page

Table 3 (continued)

Slope aspect	Flat	45	0	0
	North	217 171	365	0
	Northeast	230 838	449	0
	East	246 329	1 933	0.326 1
	Southeast	230 065	5 040	1
	South	200 051	2 768	0.510 2
	Southwest	242 198	1 944	0.328 6
	West	235 739	1 349	0.197 4
	Northwest	241 340	1 506	0.232 0
Distance from rivers	0-200 m	30 923	1 824	0.603 4
	200-400 m	30 475	2 924	1
	400-600 m	30 369	2 813	1
	600-800 m	30 269	2 319	0.881 7
	800-1 000 m	30 215	1 796	0.582 5
	1 000-1 200 m	30 201	1 428	0.453 9
	1 200-1 400 m	29 455	941	0.257 6
	1 400-1 600 m	28 366	555	0.110 9
	1 600 m	1 603 503	714	0.171 3
Distance from faults	0-500 m	197 211	2 465	0.555 2
	500-1 000 m	191 298	4 180	1
	1 000-1 500 m	175 960	4 062	1
	1 500-2 000 m	159 198	2 614	0.594 8
	2 000-2 500 m	147 609	1 438	0.282 2
	2 500-3 000 m	138 355	373	0
	3 000-3 500 m	128 098	21	0
	3 500-4 000 m	113 671	4	0
	4 000 m	592 376	197	0
Distance from roads	0-500 m	109 227	10 591	1
	500-1 000 m	83 290	3 397	0.256 4
	1 000-1 500 m	79 297	405	0
	1 500-2 000 m	79 732	462	0
	2 000-2 500 m	75 553	341	0
	2 500-3 000 m	71 192	145	0
	3 000-3 500 m	69 144	13	0
	3 500-4 000 m	67 928	0	0
	4 000 m	1 208 413	0	0
NDVI	−1-0	861 452	9 188	1
	0-0.2	448 630	5 369	0.549 3
	0.2-0.4	286 088	513	0
	0.4-0.6	233 989	262	0
	0.6-0.8	13 605	12	0
	0.8-1	7	0	0
Lithology	T	1 488 050	14 730	1
	γ5	2 624	136	0
	γδ5	104 359	0	0
	γβ5	119 284	18	0
	ηγ5	72 344	122	0
	δo5	45 955	0	0
	γρ	9 967	348	0
	γι	237	0	0
	Snow cover	1 943	0	0

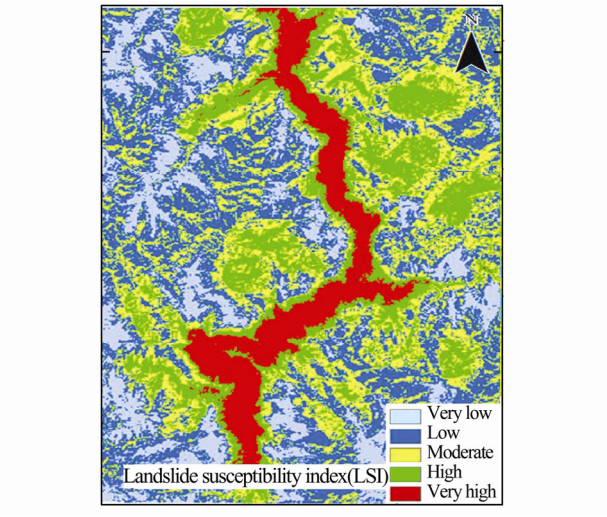

Fig. 11 Landslide susceptibility map derived from the CF model

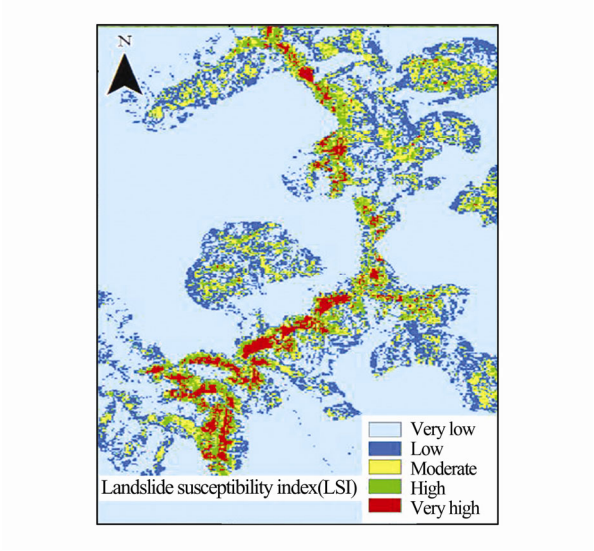

Fig. 12 Landslide susceptibility map derived from the FL model

In the present study, the LSIs of three different models were classified into five susceptibility classes as shown in Figs. 10-12 in order to simplify the results and obtain a landslide susceptibility map. The verification of the LSM was done by using ROC. The area under the ROC curve (AUC) was utilized as a comparative means to judge the performance of the models. The distribution of landslide susceptibility zones for three models were counted and the percentages in total area of five classes were presented in Table 4. Figure 13 shows the performances of the three models, in which the CF model has the best accuracy.

Table 4 Distribution of landslide susceptibility zones in landslide for AHP, CF and FL models

Landslide susceptibility classes	Percentage in total area / %		
	AHP	CF	FL
Very low	9.443	16.310	82.523
Low	27.499	34.180	6.274
Moderate	31.513	27.970	4.873
High	23.304	14.640	3.481
Very high	8.241	6.900	2.849

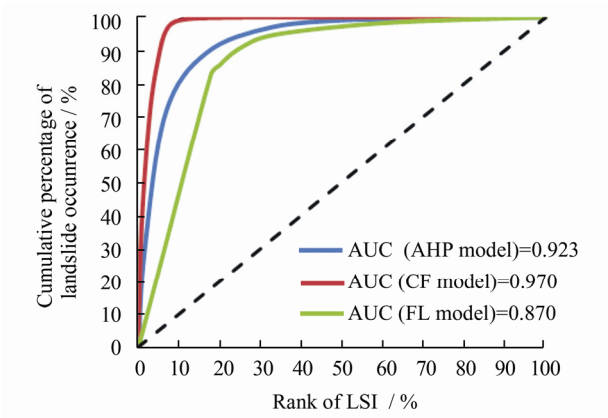

Fig. 13 Comparison of ROC curve of landslide susceptibility maps

5 Conclusion

Landslide susceptibility maps can provide the causes and controlling factors on landslide occurrence, which make it useful and effective in hazard management land planning. In this study, the susceptibility of landslides was mapped by AHP, CF and FL models. The performances of the models were analyzed by ArcGIS platform. Eight conditioning factors such as altitude, slope degree, aspect, lithology, distance from faults, distance from rivers, and NDVI were considered. For validation of landslide susceptibility maps, the ROC curves was used. In this study, a total of 75 landslides were mapped, five landslide susceptibility classes, which are very low, low, moderate, high, and very high susceptibility for landslide occurrence respectively, were classified with natural break method. The AUC plots show that the susceptibility map generated by the CF model has the highest prediction accuracy (97.0%), followed by the AHP model (92.3%) and FL model (87.0%). This indicates that the three models used in this study show good accuracy, and the CF model is the best one among the three models

in this work.

As a conclusion, these susceptibility maps can be used as a basic tool in land management and planning in landslide area. The maps help avoiding landslide susceptible regions in the study area, and similar methods can also be used where geological and topographic characteristics are the same.

References

[1] Wu W, Sidle R C. A distributed slope stability model for steep forested basins [J]. *Water Resources Research*, 1995, **31**(8): 2097-2110.

[2] Chung C J F, Fabbri A G, Van Westen C J. *Geographical Information Systems in Assessing Natural Hazards* [M]. Heidelberg: Springer-Verlag, 1995.

[3] Guzzetti F. *Landslide Hazard and Risk Assessment* [D]. Bonn: University of Bonn, 2005.

[4] Lan H X, Zhou C H, Wang L J, *et al*. Landslide hazard spatial analysis and prediction using GIS in the Xiaojiang Watershed, Yunnan, China [J]. *Engineering Geology*, 2004, **76**(1-2): 109-128.

[5] Wang W D, Xie C M, Du X G. Landslides susceptibility mapping based on geographical information system, Guizhou, south-west China [J]. *Environmental Geology*, 2009, **58**(1): 33-43.

[6] Guo C, Montgomery D R, Zhang Y, *et al*. Quantitative assessment of landslide susceptibility along the Xianshuihe fault zone, Tibetan Plateau, China [J]. *Geomorphology*, 2015, **248**: 93-110.

[7] Cao C, Wang Q, Chen J, *et al*. Landslide susceptibility mapping in vertical distribution law of precipitation area: Case of the Xulong Hydropower Station Reservoir, Southwestern China [J]. *Water*, 2016, **8**(7): 270-291.

[8] Thanh L N, Smedt F D. Application of an analytical hierarchical process approach for landslide susceptibility mapping in A Luoi district, Thua Thien Hue Province, Vietnam [J]. *Environmental Earth Sciences*, 2012, **66**(7): 1739-1752.

[9] Jebur M N, Pradhan B, Tehrany M S. Optimization of landslide conditioning factors using very high-resolution airborne laser scanning (LiDAR) data at catchment scale [J]. *Remote Sensing of Environment*, 2014, **152**: 150-165.

[10] Kayastha P, Dhital M R, De Smedt F. Application of the analytical hierarchy process (AHP) for landslide susceptibility mapping: A case study from the Tinau watershed, west Nepal [J]. *Computers & Geosciences*, 2013, **52**: 398-408.

[11] Bui D T, Tuan T A, Klempe H, *et al*. Spatial prediction models for shallow landslide hazards: A comparative assessment of the efficacy of support vector machines, artificial neural networks, kernel logistic regression, and logistic model tree [J]. *Landslides*, 2016, **13**(2): 361-378.

[12] Jia N, Mitani Y, Xie M, *et al*. Shallow landslide hazard assessment using a three-dimensional deterministic model in a mountainous area [J]. *Computers and Geotechnics*, 2012, **45**: 1-10.

[13] Hasekioğulları G D, Ercanoglu M. A new approach to use AHP in landslide susceptibility mapping: A case study at Yenice (Karabuk, NW Turkey) [J]. *Natural Hazards*, 2012, **63**(2): 1157-1179.

[14] Yilmaz I. Comparison of landslide susceptibility mapping methodologies for Koyulhisar, Turkey: Conditional probability, logistic regression, artificial neural networks, and support vector machine [J]. *Environmental Earth Sciences*, 2010, **61**(4): 821-836.

[15] Xu C, Xu X, Dai F, *et al*. Comparison of different models for susceptibility mapping of earthquake triggered landslides related with the 2008 Wenchuan earthquake in China [J]. *Computers & Geosciences*, 2012, **46**: 317-329.

[16] Devkota K C, Regmi A D, Pourghasemi H R, *et al*. Landslide susceptibility mapping using certainty factor, index of entropy and logistic regression models in GIS and their comparison at Mugling-Narayanghat road section in Nepal Himalaya [J]. *Natural Hazards*, 2013, **65**(1): 135-165.

[17] Pradhan B, Buchroithner M F. Comparison and validation of landslide susceptibility maps using an artificial neural network model for three test areas in Malaysia [J]. *Environmental & Engineering Geoscience*, 2010, **16**(2): 107- 126.

[18] Park S, Choi C, Kim B, *et al*. Landslide susceptibility mapping using frequency ratio, analytic hierarchy process, logistic regression, and artificial neural network methods at the Inje area, Korea [J]. *Environmental Earth Sciences*, 2013, **68**(5): 1443-1464.

[19] Pradhan B. A comparative study on the predictive ability of the decision tree, support vector machine and neuro-fuzzy models in landslide susceptibility mapping using GIS [J]. *Computers & Geosciences*, 2013, **51**: 350-365.

[20] Atkinson P M, Massari R. Generalised linear modelling of susceptibility to landsliding in the central Apennines, Italy [J]. *Computers & Geosciences*, 1998, **24**(4): 373-385.

[21] Reger J P. Discriminant analysis as a possible tool in landslide investigations [J]. *Earth Surface Processes and Landforms*, 1979, **4**(3): 267-273.

[22] Pourghasemi H R, Pradhan B, Gokceoglu C. Application of fuzzy logic and analytical hierarchy process (AHP) to landslide susceptibility mapping at Haraz watershed, Iran[J]. *Natural Hazards*, 2012, **63**(2): 965-996.

[23] Ermini L, Catani F, Casagli N. Artificial neural networks applied to landslide susceptibility assessment [J]. *Geomor-*

phology, 2005, **66**(1): 327-343.

[24] Yao X, Tham L G, Dai F C. Landslide susceptibility mapping based on support vector machine: A case study on natural slopes of Hong Kong, China [J]. *Geomorphology*, 2008, **101**(4): 572-582.

[25] Glade T. Linking debris-flow hazard assessments with geomorphology [J]. *Geomorphology*, 2005, **66**(1): 189-213.

[26] Qi S, Wu F, Yan F, *et al*. Mechanism of deep cracks in the left bank slope of Jinping First Stage Hydropower Station [J]. *Engineering Geology*, 2004, **73**(1): 129-144.

[27] Liu H Q, Hu R, Tan R, *et al*. Huashiban loose deposit landslide, Tiger-Leaping-Gorge, China: Analysis and prediction [J]. *Bulletin of Engineering Geology and the Environment*, 2007, **66**(2): 197-202.

[28] Wang Z L. *Research on Failure Mode and Stability Analysis of the Slope at Lenggu Hydropower Station on Yalong River* [D]. Chengdu: Chengdu University of Technology, 2016 (Ch).

[29] Saaty T L. Axiomatic foundation of the analytic hierarchy process [J]. *Management Science*, 1986, **32**(7): 841-855.

[30] Shortliffe E H, Buchanan B G. A model of inexact reasoning in medicine [J]. *Mathematical Biosciences*, 1975, **23**(3-4): 351-379.

[31] Binaghi E, Luzi L, Madella P, *et al*. Slope instability zonation: A comparison between certainty factor and fuzzy Dempster–Shafer approaches [J]. *Natural Hazards*, 1998, **17**(1): 77-97.

[32] Pourghasemi H R, Pradhan B, Gokceoglu C, *et al*. Application of weights-of-evidence and certainty factor models and their comparison in landslide susceptibility mapping at Haraz watershed, Iran [J]. *Arabian Journal of Geosciences*, 2013, **6**(7): 2351-2365.

[33] Zadeh L A. Fuzzy sets [J]. *Information and Control*, 1965, **8**(3): 338-353.

[34] Bonham-Carter G F. *Geographic Information Systems for Geoscientists*: *Modeling with GIS* [M]. Oxford: Pergamon Press, 1994.

[35] Wieczorek G F. Preparing a detailed landslide-inventory map for hazard evaluation and reduction [J]. *Bull Assoc Eng Geol*, 1984, **21**(3): 337-342.

[36] Soeters R, van Westen C J. Slope instability recognition, analysis, and zonation [J]. *Transportation Research Board Special Report*, 1996, (247): 129-177.

[37] Van Westen C J, Castellanos E, Kuriakose S L. Spatial data for landslide susceptibility, hazard, and vulnerability assessment: An overview[J]. *Engineering Geology*, 2008, **102**(3): 112-131.

[38] Kritikos T, Davies T. Assessment of rainfall-generated shallow landslide/debris-flow susceptibility and runout using a GIS-based approach: Application to western Southern Alps of New Zealand [J]. *Landslides*, 2015, **12**(6): 1051-1075.

[39] Ercanoglu M, Gokceoglu C, Van Asch T W J. Landslide susceptibility zoning north of Yenice (NW Turkey) by multivariate statistical techniques [J]. *Natural Hazards*, 2004, **32**(1): 1-23.

[40] Dai F C, Lee C F. Landslide characteristics and slope instability modeling using GIS, Lantau Island, Hong Kong [J]. *Geomorphology*, 2002, **42**(3): 213-228.

[41] Donati L, Turrini M C. An objective method to rank the importance of the factors predisposing to landslides with the GIS methodology: application to an area of the Apennines (Valnerina; Perugia, Italy) [J]. *Engineering Geology*, 2002, **63**(3): 277-289.

[42] Yalcin A, Bulut F. Landslide susceptibility mapping using GIS and digital photogrammetric techniques: A case study from Ardesen (NE-Turkey) [J]. *Natural Hazards*, 2007, **41**(1): 201-226.

[43] Korup O. Geomorphic implications of fault zone weakening: Slope instability along the Alpine Fault, South Westland to Fiordland[J]. *New Zealand Journal of Geology and Geophysics*, 2004, **47**(2): 257-267.

[44] Warr L N, Cox S. Clay mineral transformations and weakening mechanisms along the Alpine Fault, New Zealand [J]. *Geological Society*, *London*, *Special Publications*, 2001, **186**(1): 85-101.

[45] Larsen I J, Montgomery D R. Landslide erosion coupled to tectonics and river incision [J]. *Nature Geoscience*, 2012, **5**(7): 468-473.

[46] Nefeslioglu H A, Gokceoglu C, Sonmez H. An assessment on the use of logistic regression and artificial neural networks with different sampling strategies for the preparation of landslide susceptibility maps [J]. *Engineering Geology*, 2008, **97**(3): 171-191.

[47] Hall F G, Townshend J R, Engman E T. Status of remote sensing algorithms for estimation of land surface state parameters [J]. *Remote Sensing of Environment*, 1995, **51**(1): 138-156.

[48] Chen W, Li W P, Chai H C, *et al*. GIS-based landslide susceptibility mapping using analytical hierarchy process (AHP) and certainty factor (CF) models for the Baozhong region of Baoji City, China [J]. *Environmental Earth Sciences*, 2016, 75(1): 63.

□